THE JOURNAL OF PHYSICAL CHEMISTRY A

 VOLUME 112, NUMBER 37, SEPTEMBER 18, 2008

ARTICLES

Investigations of Silicon−Nitrogen Hydrides from Reaction of Nitrogen Atoms with Silane: Experiments and Calculations

Wei-Kan Chen, I-Chung Lu,† Chanchal Chaudhuri, Wen-Jian Huang, and Shih-Huang Lee*

National Synchrotron Radiation Research Center (NSRRC), 101 Hsin-Ann Road, Hsinchu Science Park, Hsinchu 30076, Taiwan

Received: May 20, 2008

Using a quadrupole mass filter and vacuum-ultraviolet ionization, we measured the time-of-flight spectra of species at mass-to-charge ratios of $m/z = 45-42$ from the reaction of N + SiH_4 in crossed molecular beams. Species with $m/z = 44$ and 43 correspond to reaction products HSiNH/$SiNH_2$ and HSiN/HNSi, respectively; species with $m/z = 45$ and 42 are assigned to isotopic variants and daughter ions, respectively, of those two reaction products. We measured the photoionization yields and branching ratios for dissociative ionization of reaction products as a function of photoionization energy. The ionization thresholds of products HSiNH/$SiNH_2$ and HSiN/HNSi were determined to be 6.7 and 9.2 eV, respectively. Furthermore, we calculated the equilibrium structures, electronic energies, and vibrational wavenumbers of various silicon−nitrogen hydrides H_xSiNH_y ($x + y = 0-3$) using quantum-chemical methods. $SiNH_2$ (X^2B_2) and HNSi ($X^1\Sigma^+$) are more stable than HSiNH (X^2A') and HSiN ($X^1\Sigma^+$) by 0.82 and 2.81 eV, respectively. $SiNH_2$ (X^2B_2), HSiNH (X^2A'), HNSi ($X^1\Sigma^+$), and HSiN ($X^1\Sigma^+$) have adiabatic ionization energies of 6.81, 8.19, 10.21, and 10.23 eV, respectively. These experimental and calculated results indicate that $SiNH_2$ (X^2B_2) and HNSi ($X^1\Sigma^+$) are dominant among isomeric products in the reaction of N + SiH_4. This work presents the first observation of products from the reaction of N + SiH_4 in crossed beams and extensive calculations on pertinent silicon−nitrogen hydrides.

I. Introduction

Carbon−nitrogen hydrides H_xCNH_y, $x + y = 1-5$, have long been investigated, but their silicon counterparts H_xSiNH_y have drawn less attention in experiments. Since the original production of iminosilicon HNSi[1] from the photolysis of azidosilane H_3SiNNN in solid argon and the much later discovery of silicon nitride SiN[2,3] in interstellar and circumstellar space and the industrial application of SiN thin films, these silicon compounds have attracted increasing attention. SiN[4−7] and iminosilicon HNSi[8−12] created in a discharge plasma of a mixture of N_2 and SiH_4 (silane) were detected by means of their spectra. By means of infrared spectra, HNSi was also identified in the gas phase[8] and again in a solid matrix.[11,12] In addition to HNSi, Maier et al.[11] detected aminosilylene $HSiNH_2$ after photolysis of H_3SiNNN in a matrix at 4 K.

Gaseous aminosilane H_3SiNH_2 persists for 1−20 h, depending on the preparation of the surfaces of its enclosure.[13] Wu[13] observed that aminosilane was produced during the mercury-sensitized photolysis of mixed SiH_4 and NH_3. With a triple-

* To whom correspondence should be addressed. Tel.: 886-3-578-0281. Fax: 886-3-578-3813. E-mail: shlee@nsrrc.org.tw.
† Department of Chemistry, National Tsing Hua University, Hsinchu 30013, Taiwan.

10.1021/jp804435y CCC: $40.75
Published on Web 08/21/2008

quadrupole mass spectrometer, aminosilane was observed also in the chemical vapor deposition (CVD) of mixed SiH_4 and NH_3.[14] Beach and Jasinski[15] and Beach[16] observed the formation of aminosilane both after irradiation of a mixture of silane and ammonia with an ArF laser and from the reaction of iodosilane with ammonia. Chen et al.[17] observed the formation of $SiNH_3$, $HSiNH_2$, and HNSi after photolysis of a mixture of Si atoms and NH_3 deposited in an Ar matrix. HNSi in interstellar space was assumed to be formed in dissociative recombination in a $[Si,N,H,H]^+$ system, which drew attention to the investigation of H_2SiN^+ and $SiNH_2^+$.[18−22] Several calculations[17−20,23−33] were devoted to the electronic energies of various silicon−nitrogen hydrides. Apart from experiments already mentioned,[17] Chen et al.[17] used density functionals of type B3LYP to calculate potential energy surfaces (PESs) for the reaction of Si (^3P, ^1D) with NH_3, including intermediates $SiNH_3$, $HSiNH_2$, H_2SiNH, and transition structures.[17] Using the Gaussian-2 (G2) method, Goldberg et al.[20] calculated the PESs of neutral and cationic systems of H_2SiN, HSiNH, and $SiNH_2$ and transition structures between isomers. Luke et al.[23] calculated the electronic energies of neutral HSiN, H_3SiN, and their isomers using the 6-31G* basis set and Moller−Plesset perturbation theory with single, double, triple, and quadruple substitution [MP4(SDTQ)]. The issue of HSiN ↔ HNSi isomerization has attracted the attention of several theoretical groups.[27−30] With the 6-31G** basis set and MP4(SDTQ) extension, Melius and Ho[24] calculated the heats of formation and enthalpies of dissociation of ground-state silicon−nitrogen hydrides. The controversy that exists about these calculations of electronic energies and assignments of symmetry of electronic states encouraged us to reinvestigate molecules of this type with the Gaussian-3 (G3) method and the coupled-cluster extension with single, double, and triple substitutions, CCSD(T).

Using a synchrotron as a source of radiation for ionization, we have detected photofragments of many types produced after photolysis of gaseous compounds,[34,35] such as for the reactions of atomic oxygen with ethene[36] and silane[37] under conditions of crossed molecular beams for which we measured the time-of-flight (TOF) spectra and photoionization yields. For instance, for oxysilanes H_xSiOH_y, $x + y = 0-3$, from the reaction of $O + SiH_4$ as a function of photoionization energy,[37] measurements of released kinetic energy indicated that reaction products H_2SiO/HSiOH, HSiO/SiOH, and SiO arose mainly from the reaction of O (^1D) with silane, whereas H_3SiO/H_2SiOH arose from the reaction of O (^3P) with silane. The measured ionization thresholds of reaction products correspond to the ionization energies of hydroxyl species H_2SiOH, HSiOH, and SiOH. Photoionization of oxysilanes resulted in dissociation. The channel for elimination of H_2 has a larger branching ratio than that for elimination of H from H_3SiO^+/H_2SiOH^+, whereas the channel for elimination of H has a larger branching ratio than that for elimination of H_2 from $H_2SiO^+/HSiOH^+$, which is interpretable according to enthalpies of reactions. Our success with the $O + SiH_4$ reaction encouraged our extensive investigation of the analogous reaction $N + SiH_4$, which we undertook under conditions of crossed molecular beams with a mass spectrometer and vacuum-ultraviolet (VUV) ionization.

II. Experiments

We conducted the title reaction using an apparatus of crossed molecular beams[34−37] that comprises two source chambers (SC1 and SC2), a reaction chamber, and a detection chamber. The two source chambers generated an atomic beam and a molecular beam that intersected each other at a right angle in the reaction chamber. The source assembly can be rotated from −20° to 110° with respect to the detector. A solenoid valve (Even-Lavie) associated with an electric discharge[38] served to generate N atoms in SC1. A mixture of N_2 (3%) in He was expanded through the Even-Lavie valve with a backing pressure 100 psi. Electric pulses (−800 V and 10 μs) were applied to the inner electrode, whereas the outer electrode was grounded. N atoms had a Gaussian-like velocity distribution with a most probable velocity 1920 m s^{-1} and a full width at half-maximum of 320 m s^{-1}. Another Even-Lavie valve installed in SC2 served to generate a molecular beam of SiH_4 that had a most probable velocity of 800 m s^{-1} at a stagnation pressure of 70 psi. Atomic N collided with SiH_4 in the reaction chamber with a collision energy of 5.0 kcal mol^{-1}. After motion along a trajectory of length 100.5 mm, reaction products were ionized with VUV radiation from an undulator. To suppress photons at high harmonics, the undulator radiation was focused into a windowless gas cell, filled with noble gas at a pressure of 10 Torr. An additional optical filter (MgF_2) served to absorb residual high-harmonic photons effectively when photons of energy less than 10 eV were desired. The undulator radiation was refocused into the ionization region of the molecular-beam apparatus. Product cations at a specified mass-to-charge ratio (m/z) were extracted with ion optics into a quadrupole mass filter. An ion counter of Daly type associated with a multichannel scaler (MCS) served to sample product ions into 1000 bins, each of duration 3 μs. We accumulated each TOF spectrum for $(4-20) \times 10^4$ pulses at a laboratory scattering angle of $\Theta = 40°$ to yield a satisfactory signal-to-noise ratio; Θ denotes the angle between the incident direction of N atoms and the detection axis.

III. Calculations

We employed density functionals of B3LYP type to optimize the equilibrium structures at the 6-311+G(d,p) level and employed a 6-311++G(3df,2p) basis set and CCSD(T) coupled-cluster routines to calculate electronic energies at optimized geometries for 17 neutral species and 18 cationic species with formulas H_xSiNH_y, $x + y = 0-3$. We calculated the vibrational wavenumbers of all normal modes and zero-point energies (ZPEs) at the B3LYP/6-311+G(d,p) level. We confirmed the electronic energies of these neutral and cationic species with the G3 and G3B3 methods. All calculations were performed with Gaussian 03 software on a computer with four CPUs and 16 GB of memory.

IV. Results and Discussion

A. Crossed-Beam Experiments. We observed the two products HSiNH/$SiNH_2$ and HSiN/HNSi that we associate with the reactions

$$N(^2D) + SiH_4 \rightarrow HSiNH/SiNH_2 + 2H \quad \Delta H = -9.8/-28.7 \text{ kcal mol}^{-1} \quad (1a/1b)$$

$$\rightarrow HSiN/HNSi + H_2 + H \quad \Delta H = -24.8/-89.7 \text{ kcal mol}^{-1} \quad (2a/2b)$$

Here, ΔH denotes the enthalpy change for reaction at 0 K between ground-state products calculated at the CCSD(T)/6-311++G(3df,2p) level; equilibrium structures and ZPEs were calculated at the B3LYP/6-311+G(d,p) level. For the reaction of atomic N with SiH_4, Figure 1 shows mass spectra of species with $m/z = 45-42$ recorded at $\Theta = 40°$. Figure 1a shows the TOF spectrum of product HSiNH/$SiNH_2$ detected with a photoionization energy of 7.4 eV. When the photoionization

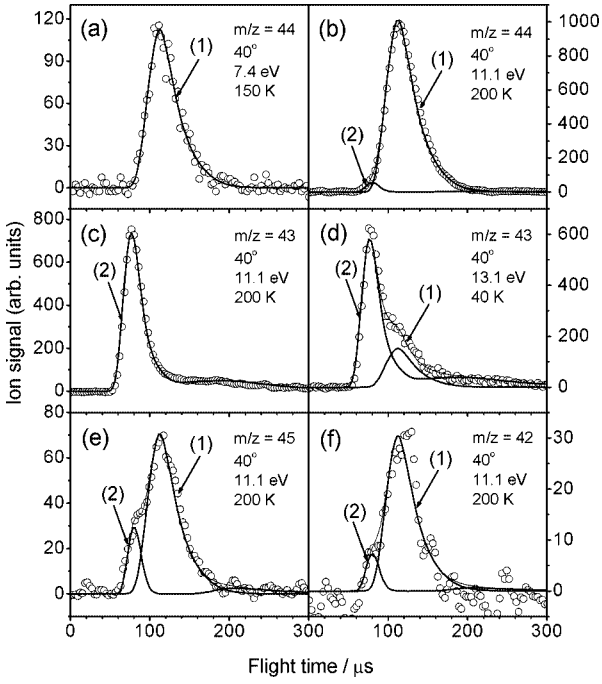

Figure 1. TOF spectra of species with $m/z = 45-42$. Each panel shows the m/z value, the laboratory scattering angle, the photoionization energy, and the accumulation number. (a) $H^{28}SiNH/^{28}SiNH_2$ from reactions 1a/1b; (b) additional rapid component $H^{29}SiN/HN^{29}Si$ from reactions 2a/2b; (c) $H^{28}SiN/HN^{28}Si$ from reactions 2a/2b; (d) additional slow component from the dissociative ionization of $H^{28}SiNH/^{28}SiNH_2$ from reactions 1a/1b; (e) rapid and slow features attributed to products $H^{30}SiN/HN^{30}Si$ and $H^{29}SiNH/^{29}SiNH_2$ from reactions 1a/1b, respectively; (f) rapid and slow features attributed to the dissociative ionization of products $H^{28}SiN/HN^{28}Si$ and $H^{28}SiNH/^{28}SiNH_2$, respectively.

energy was increased to 11.1 eV, a rapid component peaking at ~80 μs appeared at $m/z = 44$, as shown in Figure 1b; the rapid component is attributed to the ^{29}Si isotopic variant of the HSiN/HNSi product for which the TOF spectrum is shown in Figure 1c. At a photoionization energy of 11.1 eV, the ratio between the ion signal of $H^{29}SiN/HN^{29}Si$ and that of $H^{28}SiN/HN^{28}Si$ is near the 0.051 ratio of ^{29}Si and ^{28}Si in natural abundance.[39] When the photoionization energy was increased to 13.1 eV, a slow component with a maximum at ~110 μs appeared at $m/z = 43$, as shown in Figure 1d. This slow feature has a TOF distribution similar to that of the $HSiNH/SiNH_2$ product and is thus attributed to daughter ions $HSiN^+/HNSi^+$ from the dissociative ionization of this product. Panels e and f of Figure 1 exhibit bimodal TOF distributions for species with $m/z = 45$ and 42, respectively, detected at a photoionization energy of 11.1 eV. The rapid and slow features for $m/z = 45$ are attributed to ^{30}Si and ^{29}Si isotopic variants of products HSiN/HNSi and $HSiNH/SiNH_2$, respectively. At a photoionization energy of 11.1 eV, the ratio between the ion signals of $H^{30}SiN/HN^{30}Si$ and $H^{28}SiN/HN^{28}Si$ ($H^{29}SiNH/^{29}SiNH_2$ and $H^{28}SiNH/^{28}SiNH_2$) is near the 0.034 (0.051) value for the natural abundances of ^{30}Si (^{29}Si) and ^{28}Si.[39] In contrast, the rapid and slow features with $m/z = 42$ are attributed to daughter ions SiN^+ from dissociative ionization of HSiN/HNSi and $HSiNH/SiNH_2$, respectively. As ^{15}N and D atoms occur in natural abundance to extents of only 3.7×10^{-3} and 1.5×10^{-4} relative to those of ^{14}N and H,[39] respectively, we neglected their contributions in this work.

We measured the TOF spectra of species with $m/z = 45-42$ at a scattering angle of 40° with photoionization energies from 6.5 to 15 eV and an increment of ~0.2 eV. Although the

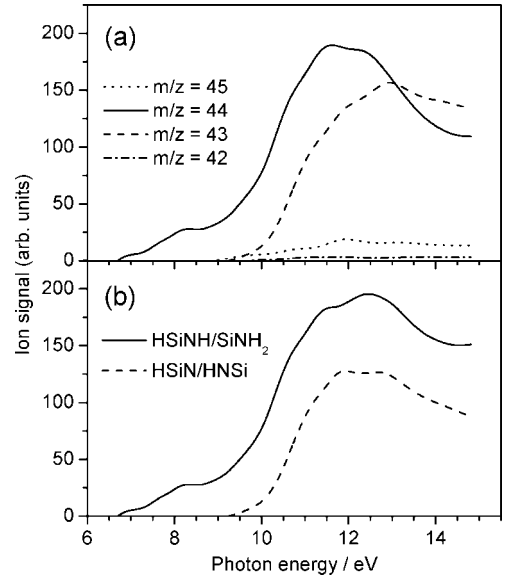

Figure 2. (a) Signals of product ions versus photionization energy. Dotted, solid, dashed, and dash−dotted lines denote experimental data for $m/z = 45-42$, respectively. The increment of photon energy is ~0.2 eV. The variation of photon flux with photon energy was uncorrected. (b) Total ion signals of products $H^{28}SiNH/^{28}SiNH_2$ and $H^{28}SiN/HN^{28}Si$ after summing of parent and daughter ions.

variation of photon flux with photon energy was uncorrected, the ratios of ion signals among these four species were conserved. Figure 2a shows the ion signals, integrated from 0 to 300 μs, of $m/z = 45-42$ versus photoionization energy. Species with $m/z = 45-42$ appear at energies of 9.0, 6.7, 9.2, and 9.8 eV, respectively. The intensity of the ion signal has a trend with respect to m/z values of 44 > 43 > 45 > 42 for a photon energy less than 13 eV, but the signal of $m/z = 43$ becomes dominant for photon energies larger than 13 eV. As each TOF spectrum likely has two components, as shown in Figure 1, we partitioned the TOF spectra and summed signals of parent and daughter ions to obtain the total ion signals of the reaction products. Figure 2b shows the total photoionization yield spectra of the reaction products $HSiNH/SiNH_2$ and HSiN/HNSi. $HSiNH/SiNH_2$ has an ionization threshold at 6.7 eV, which is near the computed adiabatic ionization energy of 6.81 eV for $SiNH_2$ ($^2B_2$) but much less than the adiabatic ionization energies of 8.19 eV for HSiNH ($^2A'$) and 9.69 eV for H_2SiN ($^2B_2$). Furthermore, from the TOF spectra of $HSiNH/SiNH_2$, we evaluated the total released kinetic energy, E_t, to have a maximum probability at 4 kcal mol^{-1}, but extending to 26 kcal mol^{-1}, which is larger/smaller than the energetic limits of 14.8/33.7 kcal mol^{-1} for reactions 1a/1b, respectively; the average released kinetic energy is ~8 kcal mol^{-1}. The $H_2SiN + 2H$ product channel is energetically inaccessible for the reaction $N(^2D) + SiH_4$ with a collision energy of 5.0 kcal mol^{-1}. $SiNH_2$, which is 18.9 kcal mol^{-1} more stable than HSiNH, presumably has a higher yield than HSiNH. Moreover, HSiNH, if produced, might have an average internal energy of ~6.8 kcal mol^{-1} that could not decrease the ionization threshold from 8.19 to 6.7 eV. In contrast, the HSiN/HNSi product has an ionization threshold at 9.2 eV that is ~1 eV less than the calculated adiabatic ionization energies of HSiN ($^1\Sigma^+$) and HNSi ($^1\Sigma^+$). Because products with a small center-of-mass kinetic energy typically have large internal energies, the TOF distribution of HSiN/HNSi alters with photoionization energy in the range of 9.2−11 eV; at a photoionization energy of 9.2 eV, the TOF spectrum has a maximum intensity, albeit small, at about 110

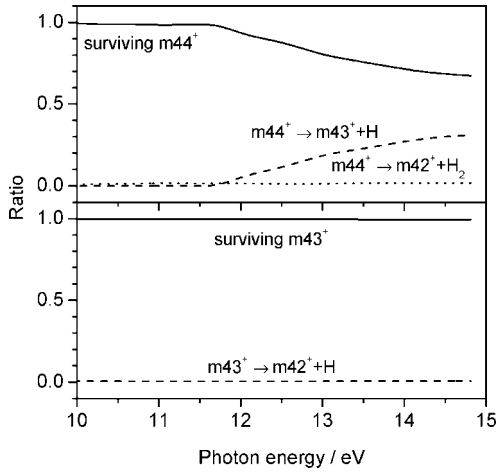

Figure 3. Branching ratios for dissociative ionization of HSiNH/$SiNH_2$ and HSiN/HNSi. $m44^+$, $m43^+$, and $m42^+$ represent $HSiNH^+/SiNH_2^+$, $HSiN^+/HNSi^+$, and SiN^+, respectively.

μs (not shown here). From the TOF spectra of HSiN/HNSi, we evaluated the released kinetic energy to have a maximum probability at 22 kcal mol^{-1}, extending to 95 kcal mol^{-1}, which is the energetic limit of reaction 2b; the average kinetic energy release is ~30 kcal mol^{-1}. Moreover, HSiN is 64.9 kcal mol^{-1} less stable than HNSi and thus has a lower yield than HNSi. Products HNSi and H_2 share an average internal energy of 65 kcal mol^{-1}. The internal energy of HNSi might decrease the ionization threshold from ~10.2 to 9.2 eV.

Figure 1 indicates that fragmentation occurred upon photoionization of the products HSiNH/$SiNH_2$ and HSiN/HNSi. Figure 3a shows the branching ratios for the dissociative ionization of HSiNH/$SiNH_2$ to $HSiN^+/HNSi^+ + H$ and to $SiN^+ + H_2$ as a function of photoionization energy. The channel to eliminate H has a threshold at ~11.7 eV that is 0.25 eV less than the enthalpy of the reaction $SiNH_2$ ($^2B_2$) → $HNSi^+$ ($^2\Pi$) + H + e^- and 2.27 eV less than that for HSiNH ($^2A'$) → $HSiN^+$ ($^2\Pi$) + H + e^-, but 0.57 eV larger than that for HSiNH ($^2A'$) → $HNSi^+$ ($^2\Pi$) + H + e^-. The dominant isomer, $SiNH_2$, has an average internal energy of ~1.11 eV that might decrease the threshold of the dissociative ionization $SiNH_2$ → $HNSi^+$ + H + e^- from 11.95 to 11.7 eV. Moreover, the full bandwidth at half-maximum of ~0.4 eV for the photoionization energy might diminish the threshold of dissociative ionization to some extent. In contrast, the channel to eliminate H_2 has a branching ratio of only 0.01−0.016 because the enthalpy of formation of SiN^+ ($^3\Sigma^-$) + H_2 is 0.77 eV larger than that for $HNSi^+$ ($^2\Pi$) + H regardless of barriers. Figure 3b shows the branching ratio for the dissociative ionization of HSiN/HNSi to SiN^+ + H as a function of photoionization energy. The branching ratio of only 0.003−0.007 in the 10−15 eV range is attributed to the large enthalpies of reaction of 5.16 eV for $HNSi^+$ ($^2\Pi$) → SiN^+ ($^3\Sigma^-$) + H and 2.32 eV for $HSiN^+$ ($^2\Pi$) → SiN^+ ($^3\Sigma^-$) + H. Although the thresholds for the dissociative ionization of HNSi ($^1\Sigma^+$) and HSiN ($^1\Sigma^+$) are larger than 15.4 and 12.6 eV, respectively, vestigial photons at high harmonics in the ionizing photon beam might decompose HSiN/HNSi following ionization.

B. Quantum-Chemical Calculations. Table 1 lists the total electronic energies, relative energies, and vibrational wavenumbers of neutral and cationic H_xSiNH_y, $x + y = 0-3$. Because electronic energies calculated with the G3B3 approach are near those calculated with the G3 method, with deviations of only between −0.003 and 0.009 hartree, we omit the G3B3 values here. From the energy differences between neutral and cationic ground states computed with the CCSD(T)/6-311++G(3df,2p)//B3LYP/6-311+G(d,p) method, we calculated the adiabatic ionization energies (IEs) of SiN ($^2\Sigma^+$), HSiN ($^1\Sigma^+$), HNSi ($^1\Sigma^+$), H_2SiN ($^2B_2$), HSiNH ($^2A'$), $SiNH_2$ ($^2B_2$), H_2SiNH ($^1A'$), $HSiNH_2$ ($^1A'$), and $SiNH_3$ ($^3A''$) to be 10.03 (10.23), 10.23 (10.39), 10.21 (10.32), 9.69 (9.95), 8.19 (8.23), 6.81 (6.86), 9.16 (9.29), 8.43 (8.59), and 6.44 (6.50) eV, respectively. The numbers within parentheses are ionization energies calculated with the G3 method, which are 0.04−0.26 eV larger than the CCSD(T) values. We adopt the CCSD(T) values for discussion. Figures 4 and 5 show the equilibrium structures of these neutral and cationic silicon−nitrogen hydrides, respectively. For a symmetric species, the redundant values for the bond length and angles are omitted. Some angles and all dihedral angles are shown in the forms ∠X−Y−Z and ∠W−X−Y−Z, respectively.

As in previous calculations,[20,24] we found the electronic ground state of SiN to be of type $^2\Sigma^+$. We found the three low-lying electronic states $^3\Sigma^-$, $^3\Pi$, and $^1\Sigma^+$ for SiN^+; state $^3\Sigma^-$ is more stable than states $^3\Pi$ and $^1\Sigma^+$ by 0.15 and 0.95 eV, respectively, and was thus assigned as the ground state of SiN^+. Using the multireference double-excitation configuration interaction (MRD-CI) method, Bruna et al.[40] found the $^3\Sigma^-$ state to be of minimum energy, consistent with our result. In contrast, Goldberg et al.[20] reported for SiN^+ the two high-lying electronic states $^1\Sigma^+$ and $^3\Sigma^+$ rather than the $^3\Sigma^-$ ground state; the $^1\Sigma^+$ and $^3\Sigma^+$ states lie 10.82 and 13.17 eV, respectively, above the $^2\Sigma^+$ state of SiN. A failure to characterize the $^3\Sigma^-$ state would give a misleading (overestimated) ionization energy of SiN. Excited state $^3\Pi$ of SiN^+ has a smaller bond length and a larger vibrational wavenumber than ground state $^3\Sigma^-$, which is attributed to the excitation of an electron from the highest occupied orbital σ to the lowest unoccupied orbital π that prefers a shorter bond. Convergence of the optimization calculation toward the energy minima of states $^3\Pi$ and $^3\Sigma^-$ requires care. With initial estimates of 1.3 and 2.0 Å for the Si−N bond length, the optimization for triplet SiN^+ converges to states $^3\Pi$ and $^3\Sigma^-$, respectively, whereas with an initial Si−N bond length of less than 1.95 Å for geometry optimization, the calculation converges to the $^3\Pi$ state, thus obscuring the $^3\Sigma^-$ ground state.

As from previous calculations,[20,23] we found HSiN to have a linear structure for its $^1\Sigma^+$ electronic ground state but an angular structure for the first triplet state, $^3A'$, which lies 1.21 eV above the $^1\Sigma^+$ state. Of the $^2\Pi$ and $^2\Sigma^+$ electronic states of $HSiN^+$, the $^2\Sigma^+$ state lies 0.91 eV above the $^2\Pi$ state. The $^2\Pi$ ($^2\Sigma^+$) state has equilibrium lengths 1.487 and 1.632 Å (1.476 and 1.518 Å) for the H−Si and Si−N bonds, respectively. Like SiN^+ ($^3\Sigma^-$ and $^3\Pi$), optimization of the geometries and electronic energies of states $^2\Sigma^+$ and $^2\Pi$ is intricate. The upper panel of Figure 6 shows the PESs of $HSiN^+$ along the Si−N bond for states $^2\Pi$ and $^2\Sigma^+$ calculated at the B3LYP/6-311++G(3df,2p) level. When the PES scan is started at a Si−N bond length 1.3 Å, the geometry optimization initially follows the $^2\Sigma^+$ PES, but transfers abruptly to state $^2\Pi$ when the Si−N bond length reaches 1.825 Å. The energy difference between the lowest unoccupied orbital (σ) and the highest occupied orbital (π) decreases monotonically with increasing Si−N bond length, and the order of energies reverses, i.e., the π orbital becomes the lowest unoccupied orbital, for bond lengths greater than 1.82 Å. With an initial value greater (less) than 1.38 Å for the Si−N bond, the optimization converges to the energy minimum of the $^2\Pi$ ($^2\Sigma^+$) state. This argument is also applicable for the $^3\Sigma^-$ and $^3\Pi$ states of SiN^+. Analogously, we found the two electronic states $^1\Sigma^+$ and $^3A'$ for HNSi and the two states $^2\Pi$ and $^2\Sigma^+$ for $HNSi^+$. The $^3A'$ state lies 3.49 eV above the $^1\Sigma^+$ electronic ground state. The $^2\Pi$ ($^2\Sigma^+$) state has equilibrium lengths of 1.664

TABLE 1: Total Electronic Energy (hartree), Point Group, Relative Energy E_{rel},[a] and Vibrational Wavenumbers[b] of Various Neutral and Cationic Silicon−Nitrogen Hydrides

species	symmetry	G3	CCSD(T)+ZPE	E_{rel} (eV)	unscaled vibrational wavenumber (cm^{-1})
SiN ($^2\Sigma^+$)	$C_{\infty v}$	−343.958129	−343.596343	0	1177
SiN^+ ($^3\Sigma^-$)	$C_{\infty v}$	−343.582096	−343.227613	10.03	759
SiN^+ ($^3\Pi$)	$C_{\infty v}$	−343.579148	−343.222278	10.18	923
SiN^+ ($^1\Sigma^+$)	$C_{\infty v}$	−343.556873	−343.192678	10.98	1138
HSiN ($^1\Sigma^+$)	$C_{\infty v}$	−344.551232	−344.188721	0	260, 260, 1236, 2225
HSiN (^{3}A′)	C_s	−344.505780	−344.144298	1.21	566, 938, 2000
$HSiN^+$ ($^2\Pi$)	$C_{\infty v}$	−344.169243	−343.812707	10.23	265, 282, 1054, 2207
$HSiN^+$ ($^2\Sigma^+$)	$C_{\infty v}$	−344.132673	−343.779385	11.14	560, 560, 1332, 2241
HNSi ($^1\Sigma^+$)	$C_{\infty v}$	−344.655606	−344.292180	0	544, 544, 1230, 3743
HNSi (^{3}A′)	C_s	−344.520310	−344.163926	3.49	559, 870, 3462
$HNSi^+$ ($^2\Pi$)	$C_{\infty v}$	−344.276412	−343.916939	10.21	321, 378, 983, 3525
$HNSi^+$ ($^2\Sigma^+$)	$C_{\infty v}$	−344.237986	−343.875643	11.33	1105, 1105, 1348, 3597
H_2SiN ($^2B_2$)	C_{2v}	−345.150597	−344.782031	0	514, 547, 918, 1037, 2231, 2261
H_2SiN^+ ($^3A_2$)	C_{2v}	−344.785041	−344.426050	9.69	511, 604, 752, 922, 2257, 2323
H_2SiN^+ ($^1A_1$)	C_{2v}	−344.754591	−344.394151	10.55	148, 555, 724, 947, 2196, 2259
HSiNH (^{2}A′)	C_s	−345.188617	−344.825914	0	519, 615, 710, 1062, 2005, 3648
$HSiNH^+$ (^{1}A′)	C_s	−344.886074	−344.524992	8.19	207, 604, 607, 1355, 2320, 3665
$HSiNH^+$ (^{3}A″)	C_s	−344.820355	−344.459181	9.98	264, 556, 714, 835, 2075, 3444
$SiNH_2$ ($^2B_2$)	C_{2v}	−345.222192	−344.855958	0	591, 743, 841, 1586, 3513, 3593
$SiNH_2^+$ ($^1A_1$)	C_{2v}	−344.970135	−344.605810	6.81	601, 680, 959, 1550, 3447, 3516
$SiNH_2^+$ ($^3A_2$)	C_{2v}	−344.839593	−344.479898	10.23	421, 489, 634, 1543, 3363, 3460
H_3SiN ($^3A_1$)	C_{3v}	−345.737481	−345.370207	0	559, 559, 712, 923, 933, 933, 2216, 2224, 2224
H_3SiN (^{1}A′)	C_s	−345.679286	−345.310247	1.63	783*i*, 571, 776, 809, 947, 947, 2147, 2153, 2213
H_3SiN^+ (^{2}A′)	C_s	−345.317664	−344.958937	11.19	1091*i*, 196, 601, 719, 774, 850, 1959, 2002, 2298
H_2SiNH (^{1}A′)	C_s	−345.819752	−345.449901	0	568, 603, 743, 768, 999, 1121, 2197, 2290, 3586
H_2SiNH ($^1A_1$)	C_{2v}	−345.812576	−345.442887	0.19	509*i*, 475, 707, 720, 1041, 1247, 2221, 2221, 3836
H_2SiNH (^{3}A″)	C_s	−345.741545	−345.374361	2.06	488, 576, 584, 683, 832, 877, 2114, 2152, 3446
H_2SiNH^+ ($^2B_2$)	C_{2v}	−345.478258	−345.113140	9.16	283, 412, 612, 667, 876, 1050, 2277, 2340, 3605
H_2SiNH^+ (^{2}A″)	C_s	−345.451393	−345.083257	9.98	597, 683, 744, 918, 976, 1930, 2274, 2356, 3442
$HSiNH_2$ (^{1}A′)	C_s	−345.841801	−345.470708	0	603, 704, 740, 845, 971, 1604, 2002, 3552, 3644
$HSiNH_2$ (^{3}A″)	C_s	−345.774234	−345.406360	1.75	443, 447, 652, 821, 822, 1588, 2071, 3548, 3630
$HSiNH_2^+$ (^{2}A′)	C_s	−345.526061	−345.160905	8.43	520, 610, 692, 882, 991, 1576, 2126, 3485, 3577
$SiNH_3$ ($^3A_1$)	C_{3v}	−345.763756	−345.396243	0	329, 549, 549, 1218, 1652, 1652, 3456, 3566, 3566
$SiNH_3$ (^{1}A′)	C_s	−345.734280	−345.363231	0.90	333, 364, 577, 1246, 1502, 1661, 3444, 3538, 3544
$SiNH_3^+$ (^{2}A′)	C_s	−345.524929	−345.159717	6.44	81, 429, 720, 1382, 1511, 1635, 3383, 3445, 3476
H (^{2}S)		−0.501003	−0.499818	0	
H_2 ($^1\Sigma_g^+$)	$D_{\infty h}$	−1.167379	−1.160794	0	4419
N (^{4}S)		−54.564343	−54.5127028	0	
N (^{2}D)		−54.470516	−54.4124319	2.73	
SiH_4 ($^1A_1$)	T_d	−291.710037	−291.397426	0	923, 923, 923, 981, 981, 2233, 2240, 2240, 2240

[a] Electronic energy relative to the neutral electronic ground-state was calculated at the level CCSD(T)+ZPE. [b] Vibrational wavenumbers were calculated at the level B3LYP/6-311+G(d,p).

and 1.022 Å (1.516 and 1.016 Å) for the Si−N and N−H bonds, respectively. The lower panel of Figure 6 shows the PESs of $HNSi^+$ along the Si−N bond for the $^2\Pi$ and $^2\Sigma^+$ states calculated at the B3LYP/6-311++G(3df,2p) level. As in the case of $HSiN^+$, the energy ordering of the π and σ orbitals of $HNSi^+$ reverses for Si−N bond lengths greater than 1.78 Å. With an initial value for the Si−N bond greater (less) than 1.5 Å, the optimization converges to the energy minimum of the $^2\Pi$ ($^2\Sigma^+$) state. This behavior of surface transfer remains observable for $HSiN^+$ but not for $HNSi^+$ in the scanning range 1.1−2.6 Å for the Si−N bond with the small 6-311+G(d,p) basis set. Goldberg et al.[20] reported a $^2\Sigma^+$ excited state rather than the $^2\Pi$ ground state for both $HSiN^+$ and $HNSi^+$. Associated with the Renner−Teller effect,[41] the calculation predicted two vibrational wavenumbers of 265 and 282 cm^{-1} (321 and 378 cm^{-1}), listed in Table 1, for the bending mode of the $^2\Pi$ state of $HSiN^+$ ($HNSi^+$). The $^2\Pi$ state splits into two electronic states when the molecule bends; the upper PES has a larger vibrational wavenumber than the lower PES.

We calculated the ground state and two cationic states for H_2SiN, HSiNH, and $SiNH_2$. H_2SiN and $SiNH_2$ belong to the same point group, $^2B_2$, whereas HSiNH has ^{2}A′ symmetry for the electronic ground state. For H_2SiN^+, the first triplet state ($^3A_2$) is 0.86 eV more stable than the first singlet state ($^1A_1$), whereas for $HSiNH^+$ ($SiNH_2^+$), the ^{3}A″ ($^3A_2$) state lies 1.79 (3.42) eV above the ^{1}A′ ($^1A_1$) state. Ground-state H_2SiN^+ has two unpaired electrons occupying b_1 and b_2 orbitals, which yields a triplet spin multiplicity. $HSiNH^+$ in the ^{1}A′ state is flexible in its bending motion; the calculated total energy increases by only 7.75×10^{-4} hartree (G3) or 3.34×10^{-5} hartree [CCSD(T) + ZPE] as $HSiNH^+$ (^{1}A′) alters to a linear structure of class $^1\Sigma^+$. Because the N−H bond is stronger than the Si−H bond, the calculated total energy follows the trend H_2SiN > HSiNH > $SiNH_2$ for the lowest singlet, doublet, and triplet states. When the molecular structure alters from point group C_{2v} to C_s, the $^2B_2$, $^3A_2$, and $^1A_1$ states correlate adiabatically with the ^{2}A′, ^{3}A″, and ^{1}A′ states, respectively. Our calculations agree with those of Goldberg et al.,[20] who used G2 theory for electronic energies but differed in the notation for the point groups. For instance, H_2SiN ($^2B_2$), $HSiNH^+$ (^{3}A″), $SiNH_2$ ($^2B_2$), $SiNH_2^+$ ($^1A_1$), and $SiNH_2^+$ ($^3A_2$) were denoted as H_2SiN ($^2A_1$), $HSiNH^+$ (^{3}A′), $SiNH_2$ ($^2A_1$), $SiNH_2^+$ (^{1}A′), and $SiNH_2^+$ ($^3A_1$), respectively, in ref 20, which we confirmed by running the same G2 calculations as Goldberg et al.[20] According to the symmetry assignments of Goldberg et al.,[20] $HSiNH^+$ (^{3}A′)

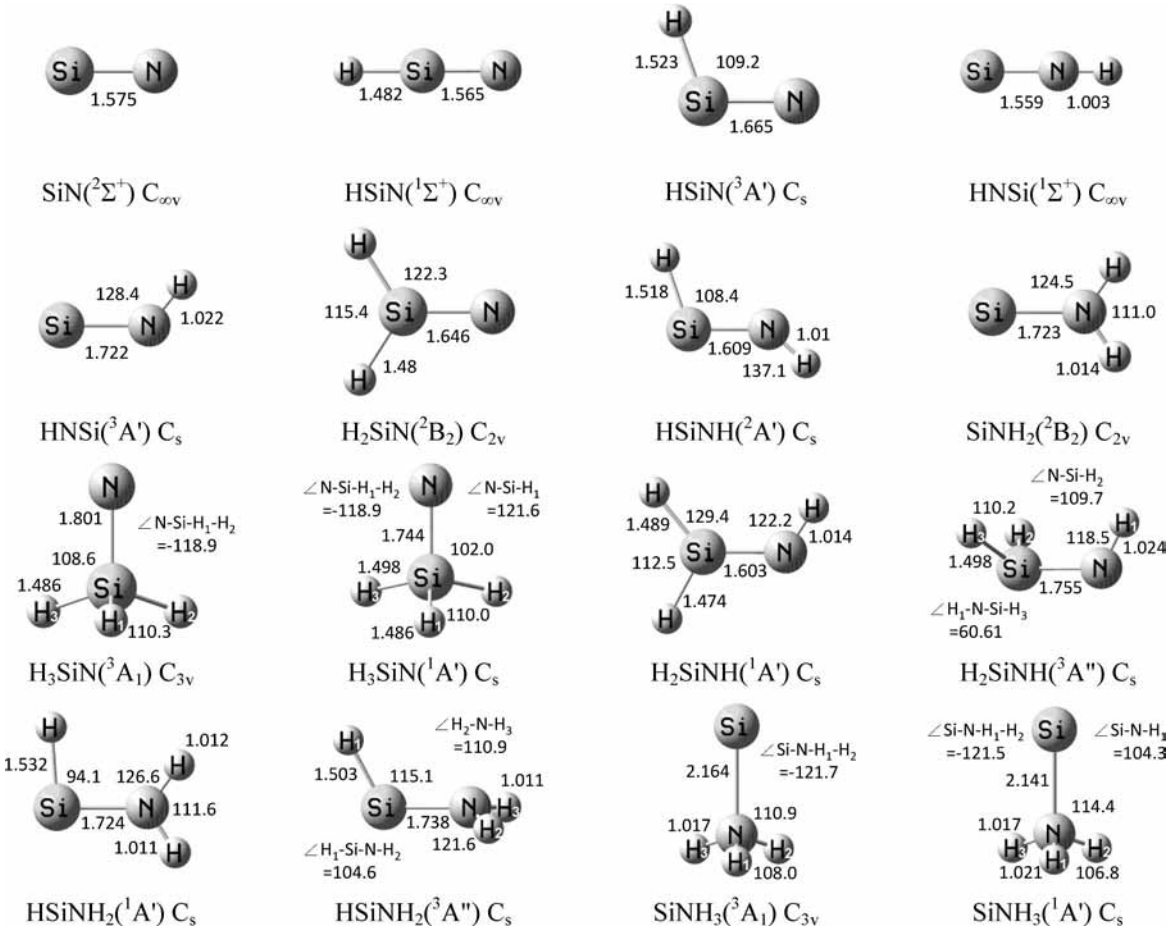

Figure 4. Equilibrium structures of various neutral silicon−nitrogen hydrides. H_3SiN ($^1A'$) is a transition structure. ∠W−X−Y−Z denotes the dihedral angle between the WXY plane and the WXZ (or XYZ) plane.

and $SiNH_2^+$ ($^3A_1$) correlated with H_2SiN^+ ($^3A_2$), which fails to conform to the rule of symmetry correlation.

Ground-state H_3SiN has two unpaired electrons occupying two doubly degenerate e orbitals localized mainly on the N atom, which gives rise to a triplet spin multiplicity. We optimized the structure of triplet H_3SiN in point group C_{3v} and assigned the ground state as $^3A_1$ but failed for singlet H_3SiN and doublet H_3SiN^+. Nevertheless, with a constraint to point group C_s, the geometry optimization converged to the $^1A'$ state for H_3SiN and to the $^2A'$ state for H_3SiN^+, although both species have an imaginary vibrational wavenumber. Calculations of the intrinsic reaction coordinate (IRC) confirmed that H_3SiN ($^1A'$) and H_3SiN^+ ($^2A'$) represent transition structures for the 1,2-H-atom exchange of H_2SiNH ($^1A'$) and H_2SiNH^+ ($^2B_2$), respectively. The rule of symmetry correlation indicates that the $^2A'$ state correlates adiabatically with the $^2B_2$ state as the molecular structure alters from point group C_s to C_{2v}. The H atom of the NH moiety migrates to the Si atom, and subsequently, one of the two H atoms originally on the SiH_2 moiety migrates to the N atom to re-form H_2SiNH. CCSD(T) calculations predicted that the barrier heights for 1,2-H-atom exchange in H_2SiNH ($^1A'$) and H_2SiNH^+ ($^2B_2$) are 3.80 and 4.19 eV, respectively. The enthalpies of reactions for H_2SiNH ($^1A'$) → H_2SiN ($^2B_2$) + H and H_2SiNH^+ ($^2B_2$) → H_2SiN^+ ($^3A_2$) + H are as large as 4.57 and 5.09 eV, respectively, which accounts for the large barriers for the 1,2-H-atom exchanges.

Luke et al.[23] reported a $^1A_1$ state of point group C_{2v} rather than a $^1A'$ ground state for H_2SiNH. From our IRC calculations, we identified H_2SiNH ($^1A_1$) as a transition structure of H_2SiNH ($^1A'$) for the Si−N−H bending motion in the molecular plane; the barrier height is only 0.19 eV. H_2SiNH ($^3A''$), the lowest triplet state, lies 2.06 eV above the $^1A'$ ground state. Figure 5 indicates that H_2SiNH^+ ($^2B_2$) has a planar structure of point group C_{2v}, whereas H_2SiNH^+ ($^2A''$) has a planar structure of point group C_s. As a $^2A''$ state correlates adiabatically with a $^2B_1$ state rather than a $^2B_2$ state as the molecular structure alters from point group C_s to C_{2v}, H_2SiNH^+ ($^2B_2$) and H_2SiNH^+ ($^2A''$) are situated on distinct PESs. As in the cases of SiN^+ ($^3\Sigma^-$, $^3\Pi$), $HSiN^+$ ($^2\Pi$, $^2\Sigma^+$), and $HNSi^+$ ($^2\Pi$, $^2\Sigma^+$), convergence of the calculation toward the equilibrium structure of the $^2A''$ state that lies 0.82 eV above the $^2B_2$ ground state ($^2A'$ in point group C_s) of H_2SiNH^+ is intricate. Under a constraint of C_s symmetry, the calculation for geometry optimization converges to the equilibrium structures of the $^2A''$ and $^2A'$ states (i.e., $^2B_2$) of H_2SiNH^+ with initial ∠Si−N−H values of less and greater than 136.6°, respectively. On scanning the PES along the coordinate of Si−N−H bending from 120° to 180° under a constraint of point group C_s, at ∠Si−N−H ≈ 143.5°, the calculated electron configuration of H_2SiNH^+ abruptly alters from the $^2A''$ to the $^2A'$ state. As for the H_2SiNH system, $HSiNH_2$ has a planar equilibrium geometry for the $^1A'$ ground state that lies 1.75 eV lower than the $^3A''$ state; Chen et al.[17] assigned the $^3A''$ state to $^3A'$. In contrast to H_2SiNH^+, in its ground state, $HSiNH_2^+$ has an equilibrium structure belonging to point group C_s rather than C_{2v}. Analogous to H_3SiN, $SiNH_3$ in its ground state has a structure with point group C_{3v} and a $^3A_1$ ground state; two unpaired electrons occupy two doubly degenerate e orbitals localized mainly on the Si atom, which yields a triplet spin multiplicity. In contrast to H_3SiN ($^1A'$) and H_3SiN^+ ($^2A'$), we found energy minima rather than transition structures for $SiNH_3$

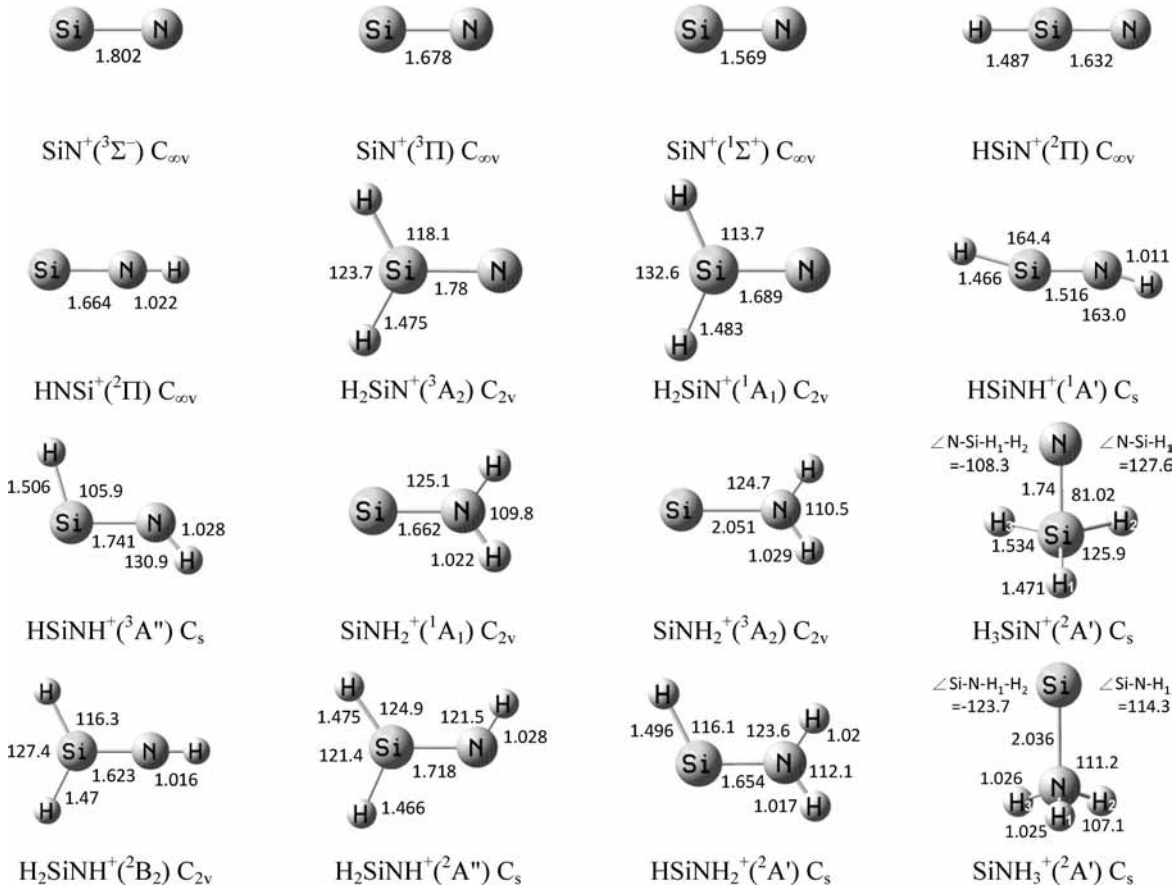

Figure 5. Equilibrium structures of various cationic silicon−nitrogen hydrides. H_3SiN^+ ($^2A'$) is a transition structure. ∠W−X−Y−Z denotes the dihedral angle between the WXY plane and the WXZ (or XYZ) plane.

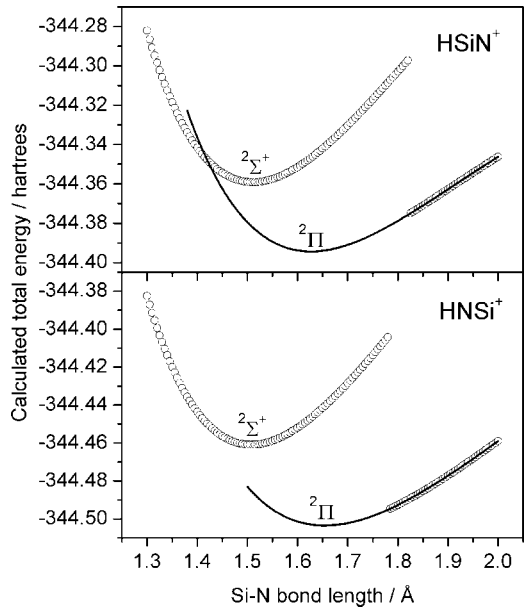

Figure 6. Scan of potential energy surfaces of $HSiN^+$ and $HNSi^+$ along the Si−N bond with method B3LYP/6-311++G(3df,2p) and of increment 0.005 Å in the Si−N bond length. The solid line and circles are for states $^2\Pi$ and $^2\Sigma^+$, respectively, for both $HSiN^+$ and $HNSi^+$.

($^1A'$) and $SiNH_3^+$ ($^2A'$) at C_s symmetry. $SiNH_3$ ($^1A'$) lies above $SiNH_3$ ($^3A_1$) in electronic energy by 0.90 eV, which is less than the value of 1.02 eV obtained by Chen et al. using B3LYP theory alone.[17]

V. Conclusion

On the basis of the first experiments on $HSiNH/SiNH_2$ and HSiN/HNSi from the reaction of atomic N with SiH_4 in crossed molecular beams, we propose that products of these two types arise mainly from the reaction of $N(^2D) + SiH_4$. We determined the ionization thresholds of the products $HSiNH/SiNH_2$ and HSiN/HNSi to be 6.7 and 9.2 eV, respectively. The value of 6.7 eV coincides with a calculated adiabatic IE of 6.81 eV for $SiNH_2$, whereas the value of 9.2 eV is ~1.0 eV less than the calculated adiabatic IE of HSiN and HNSi. The internally hot HNSi is responsible for the red shift in the ionization threshold. As HSiN lies 64.9 kcal mol^{-1} above HNSi, the measured distribution of kinetic energy favors HNSi over HSiN as the major product. A portion of $HSiNH/SiNH_2$ decomposes to $HSiN^+/HNSi^+ + H$ following photoionization with a threshold of about 11.7 eV. In contrast, the extent of dissociative ionization of $HSiNH/SiNH_2$ to $SiN^+ + H_2$ is low, indicating a large dissociation threshold. Similarly, the large enthalpies of the reactions $HSiN^+/HNSi^+ \rightarrow SiN^+ + H$ hinder the dissociative ionization of HSiN/HNSi. Our present work has yielded the first measurements of TOF distributions, photoionization yields, and dissociative ionizations of $HSiNH/SiNH_2$ and HSiN/HNSi. In a future work, we shall present kinetic energy and spatial angular distributions of products and describe the dynamics of reaction $N + SiH_4$ based on a calculated PES.

We calculated the electronic energies and vibrational wavenumbers for silicon−nitrogen hydrides with H_xSiN_y, $x + y = 0-3$. Optimization of the geometries and electronic energies of SiN^+ ($^3\Sigma^-$, $^3\Pi$), $HSiN^+$ ($^2\Pi$, $^2\Sigma^+$), and $HNSi^+$ ($^2\Pi$, $^2\Sigma^+$) requires care: With a short Si−N bond as an initial value, the

optimization converges toward an electronic excited state rather than the ground state. For H_2SiNH^+ ($^2B_2$, $^2A''$), the optimization with a small initial value for the ∠Si−N−H angle converges toward the $^2A''$ electronic excited state rather than the $^2B_2$ ground state. The present calculations correct previous assignments of electronic states and provide useful molecular parameters for neutral and cationic silicon−nitrogen hydrides that might occur in the $N + SiH_4$ reaction.

Acknowledgment. The National Synchrotron Radiation Research Center, Academia Sinica, and National Science Council of Taiwan (Grant NSC96-2113-M-213-001) provided support for this research.

References and Notes

(1) Ogilvie, J. F.; Cradock, S. *Chem. Commun.* **1966**, *12*, 364.
(2) Turner, B. E. *Bull. Am. Astron. Soc.* **1991**, *23*, 933.
(3) Turner, B. E. *Astrophys. J.* **1992**, *388*, L35.
(4) Turner, B. E. *Astrophys. J.* **1991**, *376*, 573.
(5) Turner, B. E. In *Astrochemistry of Cosmic Phenomena*; Singh, P. D., Ed.; Kluwer: Dordrecht, The Netherlands, 1992; p 181. Glassgold, A. E. In *Astrochemistry of Cosmic Phenomena*; Singh, P. D., Ed.; Kluwer: Dordrecht, The Netherlands, 1992; p 379.
(6) Saito, S.; Endo, Y.; Hirota, E. *J. Chem. Phys.* **1983**, *78*, 6447.
(7) Yamada, C.; Hirota, E. *J. Chem. Phys.* **1985**, *82*, 2547.
(8) Elhanine, M.; Farrenq, R.; Guelachvili, G. *J. Chem. Phys.* **1991**, *94*, 2529.
(9) Bogey, M.; Demuynck, C.; Destombes, J. L.; Walters, A. *Astron. Astrophys.* **1991**, *244*, L47.
(10) Botschwina, P.; Tommek, M.; Sebald, P.; Bogey, M.; Demuynck, C.; Destombes, J. L.; Walters, A. *J. Chem. Phys.* **1991**, *95*, 7769.
(11) Maier, G.; Glatthaar, J.; Reisenauer, H. P. *Chem. Ber.* **1989**, *122*, 2403.
(12) Maier, G.; Glatthaar, J. *Angew. Chem.* **1994**, *106*, 486; *Angew. Chem., Int. Ed. Engl.* **1994**, *33*, 473.
(13) Wu, C.-H. *J. Phys. Chem.* **1987**, *91*, 5054.
(14) Smith, D. L.; Alimoda, A. S.; Chen, C. C.; Jackson, W.; Wacker, B. *Mater. Res. Soc. Symp. Proc.* **1988**, *118*, 107.
(15) Beach, D. B.; Jasinski, J. M. *J. Phys. Chem.* **1990**, *94*, 3019.
(16) Beach, D. B. *Inorg. Chem.* **1992**, *31*, 4174.
(17) Chen, M.; Zheng, A.; Lu, H.; Zhou, M. *J. Phys. Chem. A* **2002**, *106*, 3077.
(18) Parisel, O.; Hanus, M.; Ellinger, Y. *J. Chem. Phys.* **1996**, *104*, 1979.
(19) Parisel, O.; Hanus, M.; Ellinger, Y. *J. Phys. Chem.* **1996**, *100*, 2926.
(20) Goldberg, N.; Hrusak, J.; Iraqi, M.; Schwarz, H. *J. Phys. Chem.* **1993**, *97*, 10687.
(21) Herbst, E.; Millar, T. J.; Wlodek, S.; Bohme, D. K. *Astron. Astrophys.* **1989**, *205*, 222.
(22) Langer, W. D. *Astrophys. J.* **1990**, *123*, 352.
(23) Luke, B. T.; Pople, J. A.; Krogh-Jespersen, M. B.; Apeloig, Y.; Karni, M.; Chandrasekhar, J.; Schleyer, P. v. R. *J. Am. Chem. Soc.* **1986**, *108*, 270.
(24) Melius, C. F.; Ho, P. *J. Phys. Chem.* **1991**, *95*, 1410.
(25) Hendewerk, M. L.; Frey, R.; Dixon, D. A. *J. Phys. Chem.* **1983**, *87*, 2026.
(26) Glidewell, C.; Thomson, C. *J. Comput. Chem.* **1983**, *4*, 9.
(27) Apeloig, Y.; Albrecht, K. *J. Am. Chem. Soc.* **1995**, *117*, 7263.
(28) Jursic, B. S. *J. Mol. Struct. (THEOCHEM)* **1998**, *455*, 77.
(29) Jursic, B. S. *J. Mol. Struct. (THEOCHEM)* **1999**, *460*, 11.
(30) Kwon, O.; Kwon, Y. *J. Mol. Struct. (THEOCHEM)* **1999**, *460*, 213.
(31) Truong, T. N.; Gordon, M. S. *J. Am. Chem. Soc.* **1986**, *108*, 1775.
(32) Botschwina, P.; Tommek, M.; Sebald, P.; Bogey, M.; Demuynck, C.; Destombes, J. L. Walters, A. *J. Chem. Phys.* **1991**, *95*, 7769.
(33) Chong, D. P.; Papousek, D.; Chen, Y.-T.; Jensen, P. *J. Chem. Phys.* **1993**, *98*, 1352.
(34) Lee, S.-H.; Lee, Y.-Y.; Lee, Y. T.; Yang, X. *J. Chem. Phys.* **2003**, *119*, 827.
(35) Lee, S.-H.; Ong, C. S.; Lee, Y. T. *J. Chem. Phys.* **2006**, *124*, 074306.
(36) Lee, S.-H.; Huang, W.-J.; Chen, W.-K. *Chem. Phys. Lett.* **2007**, *446*, 276.
(37) Chaudhuri, C.; Lu, I-C.; Lin, J. J.; Lee, S.-H. *Chem. Phys. Lett.* **2007**, *444*, 237.
(38) Lu, I-C.; Huang, W.-J.; Chaudhuri, C.; Chen, W.-K.; Lee, S.-H. *Rev. Sci. Instrum.* **2007**, *78*, 083103.
(39) Lide, D. R., Ed. *Handbook of Chemistry and Physics*, 78th ed.; CRC Press: Boca Raton, FL, 1997.
(40) Bruna, P. J.; Peyerimhoff, S. D.; Buenker, R. J. *J. Chem. Phys.* **1980**, *72*, 5437.
(41) Sari, L.; Yamaguchi, Y.; Schaefer, H. F. *J. Chem. Phys.* **2001**, *115*, 5932.

JP804435Y